Taylor & Francis
Taylor & Francis Group

BRIEF REPORT

Noninvasive monitoring of cancer therapy induced activated T cells using [18F]FB-IL-2 PET imaging

S. V. Hartimath[a], O. Draghiciu[b], S. van de Wall[b], V. Manuelli [ID][a], R. A. J. O. Dierckx[a], H. W. Nijman[c], T. Daemen[b,*], and E. F. J. de Vries [ID][a,*]

[a]Department of Nuclear Medicine and Molecular Imaging, University of Groningen, University Medical Center Groningen, the Netherlands; [b]Department of Medical Microbiology, Tumor Virology and Cancer Immunotherapy, University of Groningen, University Medical Center Groningen, the Netherlands; [c]Department of Gynecological Oncology, University of Groningen, University Medical Center Groningen, the Netherlands

ABSTRACT

Cancer immunotherapy urgently calls for methods to monitor immune responses at the site of the cancer. Since activated T lymphocytes may serve as a hallmark for anticancer responses, we targeted these cells using the radiotracer N-(4-[18F]fluorobenzoyl)-interleukin-2 ([18F]FB-IL-2) for positron emission tomography (PET) imaging. Thus, we noninvasively monitored the effects of local tumor irradiation and/or immunization on tumor-infiltrating and systemic activated lymphocytes in tumor-bearing mice. A 10- and 27-fold higher [18F]FB-IL-2 uptake was observed in tumors of mice receiving tumor irradiation alone or in combination with immunization, respectively. This increased uptake was extended to several non-target tissues. Administration of the CXCR4 antagonist AMD3100 reduced tracer uptake by 2.8-fold, indicating a CXCR4-dependent infiltration of activated T lymphocytes upon cancer treatment. In conclusion, [18F]FB-IL-2 PET can serve as a clinical biomarker to monitor treatment-induced infiltration of activated T lymphocytes and, on that basis, may guide cancer immunotherapies.

Introduction

Activation of the immune system for effective tumor control is a mainstay for the burgeoning field of cancer therapy.[1,2] Positron emission tomography (PET) could provide a pivotal platform for *in vivo* imaging of immune biomarkers that are induced upon cancer therapy and serve to replace invasive approaches of low reproducibility. However, this technology is currently limited by the paucity of clinically proven immune tracers.

Viable candidates for assessment of therapy-induced responses are activated T lymphocytes that infiltrate intratumorally for effective antitumor control. We recently developed a PET tracer, specifically binding to interleukin-2 receptors expressed on activated $CD25^+$ T cells, N-(4-[18F]-fluorobenzoyl)-interleukin-2 ([18F]FB-IL-2).[3] For potential clinical relevance, we validated the use of this probe in animal models of inflammation and demonstrated that the PET tracer shows CD25-dependent uptake in mice and rats[4,5] and is able to monitor progression of insulitis in animal models of type 1 diabetes (unpublished data). However, whether [18F]FB-IL-2 PET could be utilized as a tool to monitor cancer therapeutic responses *in vivo* remains to be established. Most immunotherapies are based on humanized antibodies and effective evaluation of such therapies is currently limited by the use of

immune-deficient preclinical models with human tumors and reconstitution of the immune system using human peripheral blood mononuclear cells. To circumvent this hurdle, PET technology may also be applied in preclinical models for assessment of endogenous immune responses induced by clinically relevant therapeutic approaches other than humanized antibodies.

For this purpose, we utilized a preclinical cervical cancer model to assess [18F]FB-IL-2 as a diagnostic tool, using local tumor irradiation and viral-vector based immunization as therapeutic strategies to induce infiltration of activated T cells. Our viral vector is based on recombinant Semliki Forest virus (rSFV) encoding a fusion protein of E6 and E7 derived from human papilloma virus (HPV) type 16 (rSFVeE6,7).[6] In combination with local irradiation, immunization with rSFVeE6,7 in tumor-bearing mice demonstrated a synergistic antitumor effect.[7] These synergistic effects culminates from mechanisms such as trafficking of activated tumor-infiltrating lymphocytes (TILs) to the tumor site, upregulation of tumor antigens for TIL recognition and induction of positive immune modulatory pathways.[8-13]

In this report, we validated [18F]FB-IL-2 PET as a noninvasive imaging tool for monitoring CD25-expressing, activated T lymphocytes in the context of clinically relevant cancer

---

CONTACT E. F. J. de Vries ✉ e.f.j.de.vries@umcg.nl 📧 Department of Nuclear Medicine and Molecular Imaging, University of Groningen, University Medical Center Groningen, 9713 GZ, Groningen, the Netherlands.

📄 Supplemental data for this article can be accessed on the publisher's website.

*These authors contributed equally to this work.

therapies. We further obtained insight into the mechanism of action of lymphocyte infiltration upon combination treatment with CXCR4 antagonist AMD3100.

Materials and methods

Cell lines

Baby hamster kidney cells (BHK-21) were obtained from the American Type Culture Collection (# CCL-10). The TC-1 cell line was created by transfection of C57Bl/6 primary lung epithelial cells with a retroviral vector that expresses the human papillomavirus 16 (HPV16) E6E7 fusion protein.[14] The cells were obtained in 1998 from Prof. Dr. Cornelis Melief (Leiden University Medical Center, Leiden, The Netherlands). Cells were cultured as described before.[6]

Animals

Specified pathogen-free female C57BL/6 mice between the age of 8 and 10 weeks (bodyweight 20.8 ± 1.9 g) were purchased from Harlan CPB (Zeist, The Netherlands) and housed according to the institute's guidelines. Mice were maintained at 12 h/12 h day/night regime and fed standard laboratory chow. The Institutional Animal Care and Use Committee approved all experiments.

Production, purification, and titer determination of SFVeE6,7 particles

SFVeE6,7 production, purification, and titer determination were performed as previously described.[15] Shortly, SFVeE6,7 particles were produced by co-electroporation of BHK-21 cells with an RNA encoding the SFV transgene (the E6E7 fusion protein), replicase, and a helper RNA encoding the structural proteins of SFV. Recombinant SFV particles produced by transfected BHK-21 cells were purified on a sucrose density gradient and titrated on BHK-21 cells using a polyclonal rabbit antireplicase (non-structural protein 3) antibody [gift from Dr. T. Ahola (Biocentre Viikki, Helsinki, Finland)].

Tumor inoculation, SFVeE6,7 immunizations, and local tumor irradiation

Mice were inoculated subcutaneously in the neck with 2×10^4 TC-1 cells suspended in 0.2 mL Hank's Balanced Salt Solution (Invitrogen, Paisley, UK). Two weeks later, TC-1 tumors were locally irradiated with a single 14 Gy radiation dosage, using the X-RAD 320 Biological Irradiator (Precision X-ray, North Branford, CT, USA) at a delivery rate of 1.64 Gy/min. Mice were anesthetized with isoflurane before irradiation and were placed in plastic constrainers to ensure immobilization for the localized irradiation of the tumor. Control animals were sham-irradiated. The following day, a group of irradiated mice was intramuscularly immunized with a single dose of 5×10^6 SFVeE6,7 particles. Another group of irradiated mice received a vehicle PBS solution. The third group of irradiated mice received the clinically approved CXCR4 antagonist

AMD3100.8HCl (Plerixafor) in a daily i.p. dosage of 3 mg/kg body weight until the end of the experiment (6 d).

[^{18}F]FB-IL-2 production

IL-2 was labeled with fluorine-18 by conjugation of the protein with succinimidyl 4-[^{18}F]-fluorobenzoate ([^{18}F]SFB) as described before, but with minor alterations.[5] [^{18}F]SFB was purified by solid phase extraction using an Oasis HLB cartridge (30 mg, 1 mL). The cartridge was washed with 5 mL of water and eluted with 5 mL of ether. The ether fraction was collected and the solvent was evaporated at 50 °C. Next, 100 μL of human recombinant IL-2 (Proleukin; Novartis) solution in nitrogen-purged water (2 mg/mL) were incubated with [^{18}F]SFB reconstituted in 100 μL of ethanol in the presence of 100 μL Tris buffer (pH = 8.5). The reaction mixture was heated at 50 °C for 10 min. The resulting product was purified by size-exclusion chromatography using a PD-10 cartridge (GE Healthcare, The Netherlands), which was previously equilibrated with approximately 25 mL elution buffer (0.05% sodium dodecylsulfate, 0.5% human serum albumin in PBS). Fifteen fractions of ∼0.5 to 0.8 mL each were collected and each fraction was analyzed by radio-thin layer chromatography, using ethyl acetate/hexane (4:1) as the eluent. The fractions containing pure [^{18}F]FB-IL-2 were pooled and used for *in vivo* imaging and *ex vivo* biodistribution studies. Quality control (QC) of [^{18}F]FB-IL-2 was performed by ultra-high performance liquid chromatography (UPLC), using an Acquity UPLC BEH-shield RP18 column \(1.7 μm, 3 × 50 mm) and gradient elution with a mixture of 0.1% aqueous trifluoroacetic acid (solvent A) and 0.1% trifluoroacetic acid in ethanol (solvent B). The following gradient profile was used: 0–1 min 5% B, 1–4 min 30% B, 4–8 min 50% B, 8–13 min 70% B and 13–15 min 5% B, at a flow rate of 0.8 mL/min. Retention times were 9.6 min for [^{18}F]FB-IL-2, 5.0 min for [^{18}F]SFB, and 4.0 min for 4-[^{18}F]fluorobenzoic acid. Radiochemical purity of [^{18}F]FB-IL-2 was always above 96%. The specific activity of the tracer was 20 ± 4 GBq/mg.

PET acquisition

Mice were anesthetized with isoflurane (5% for induction; 2% for maintenance) in medical air throughout the procedure. The animals were injected through the tail vein with 4.0 ± 2.9 MBq of [^{18}F]FB-IL-2. After tracer injection, the mice were placed in a trans-axial position in the PET camera (microPET Focus 220; Siemens Medical Solution USA) with the tumors in the center of the field of view and a dynamic PET scan was immediately acquired for 30 min (i.e., 5 min delay between tracer injection and start acquisition). After the emission scan, a transmission scan of 15 min with a Co-57 point source was obtained for the correction of attenuation and scatter by tissue. Two animals were scanned simultaneously in each scan session.

Image reconstruction and analysis

All emission scans were normalized and corrected for attenuation, scatter and radioactive decay. Emission sinograms were iteratively reconstructed in six frames of 5 min, using ordered subset expectation maximization (OSEM) algorithm with 4

iterations and 16 subsets. The regions of interest (ROIs) were manually drawn on the summed PET images (5–35 min post-injection) and subsequently the tumor was automatically delineated within the ROI using a threshold of 75% of the maximum uptake in the tumor. The average tracer uptake in the last time frame (i.e., 30–35 min post-injection) was calculated using standard software (Inveon, Siemens, USA). ROI volumes corresponded well with the tumor mass determined in the biodistribution study. Tracer uptake was expressed as percentage injected dose per gram tissue (%ID/g).

Ex vivo biodistribution

After completion of the PET scans, mice were sacrificed by cervical dislocation, and several tissues including the tumor were excised. Blood was centrifuged (5 min at 13,000 rpm) to separate cells from plasma. All tissue samples were weighed and the amount of radioactivity within each tissue sample was determined by an automated γ-counter (LKB Wallace, Finland). A small fraction of plasma and urine samples was used to test percentage of intact tracer by a tricholoracetic acid precipitation assay. [18F]FB-IL-2 tracer uptake in each organ was expressed as %ID/g.

Statistical analysis

All data are expressed as mean $\pm$ standard deviation. Statistical analyses by one-way ANOVA were performed using GraphPad Prism 5. Probability (p) values lower than 0.05 were considered statistically significant.

Results

To evaluate the feasibility of [18F]FB-IL-2 as a tool for assessment of *in vivo* tumor infiltration of activated T lymphocytes in the cancer therapy setting, we treated HPV-specific tumor-bearing mice with irradiation alone or in a combination treatment with rSFVeE6,7 immunization. Time–activity curves showed that tracer uptake in the tumor of immunized rats was slowly increasing over time, whereas it remained relatively stable for the other groups (Fig. S1). PET data acquired between 30 and 35 min after tracer injection revealed accumulation of [18F]FB-IL-2 in TC-1 tumors of all animals (Fig. 1A–E). [18F]FB-IL-2 tumor uptake was 10-fold higher in the group receiving a single 14 Gy irradiation dosage (3.4 ± 0.7 %ID/g) when compare with the sham-irradiated control group (0.34 ± 0.16 %ID/g, $p < 0.01$).

Upon combination of 14 Gy local tumor irradiation with SFVeE6,7 immunization, intra-tumoral [18F]FB-IL-2 uptake
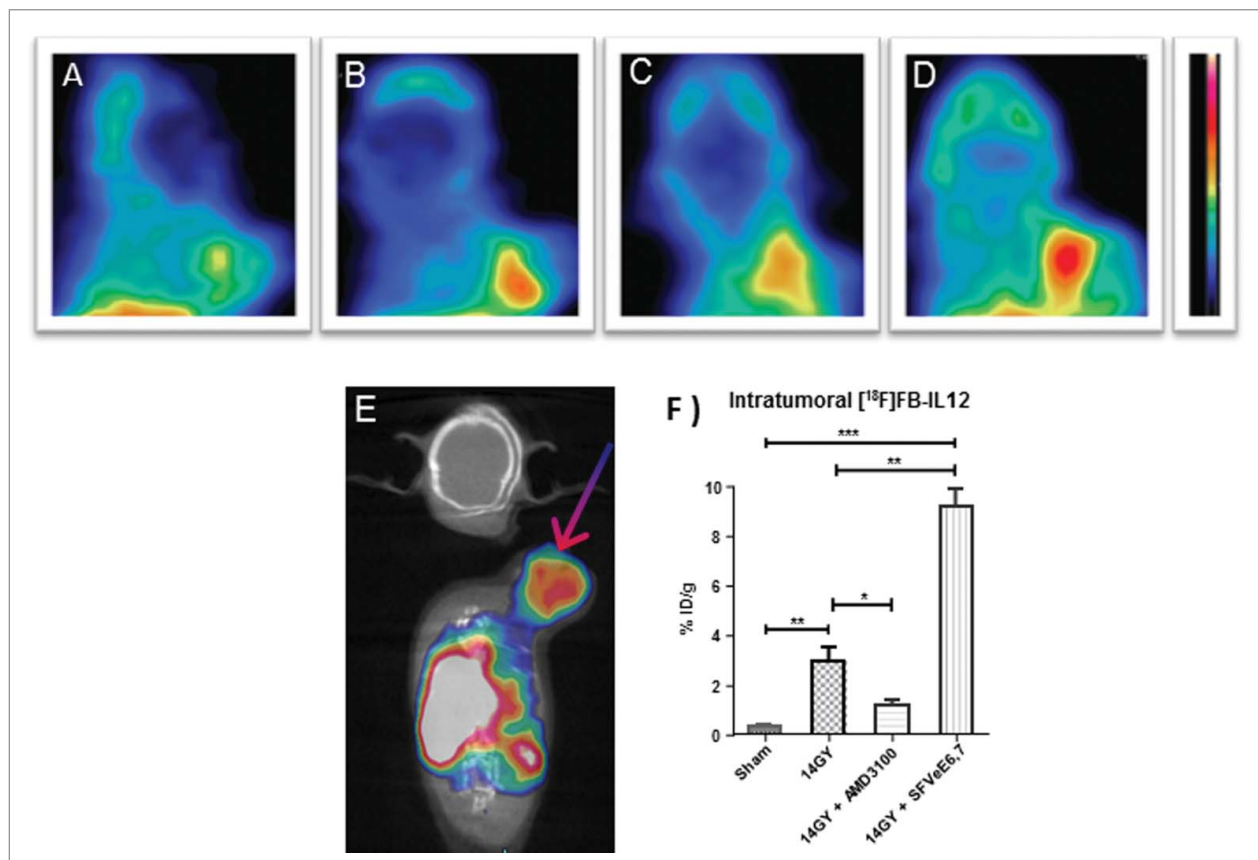

Figure 1. *In vivo* PET imaging and quantitative uptake of [18F]FB-IL-2 in TC-1 tumors. Representative cross-sectional images of TC-1 tumor-bearing mice with the tumor in the field of view. Mice were subjected to different treatments: (A) sham-irradiation (control), (B) 14 Gy local tumor irradiation, (C) 14 Gy local tumor irradiation followed by administration of the CXCR4 antagonist AMD3100 or (D) 14 Gy local tumor irradiation followed by immunization with 5×10^6 SFVeE6,7 particles. (E) Representative a fused PET and computer tomography (CT) image of a cross-section of a TC-1 tumor bearing mouse treated with 14 Gy local tumor irradiation followed by immunization with SFVeE6,7 particles. (F) Quantitative estimation of the *in vivo* tracer uptake, expressed as percentage of the injected tracer dose per gram of tissue (%ID/g). Arrow indicates the position of the tumor, and all the data represent the mean $\pm$ standard deviation. Statistically significant differences between groups are indicated by $^*p < 0.05$, $^{**}p < 0.01$, and $^{***}p < 0.001$.
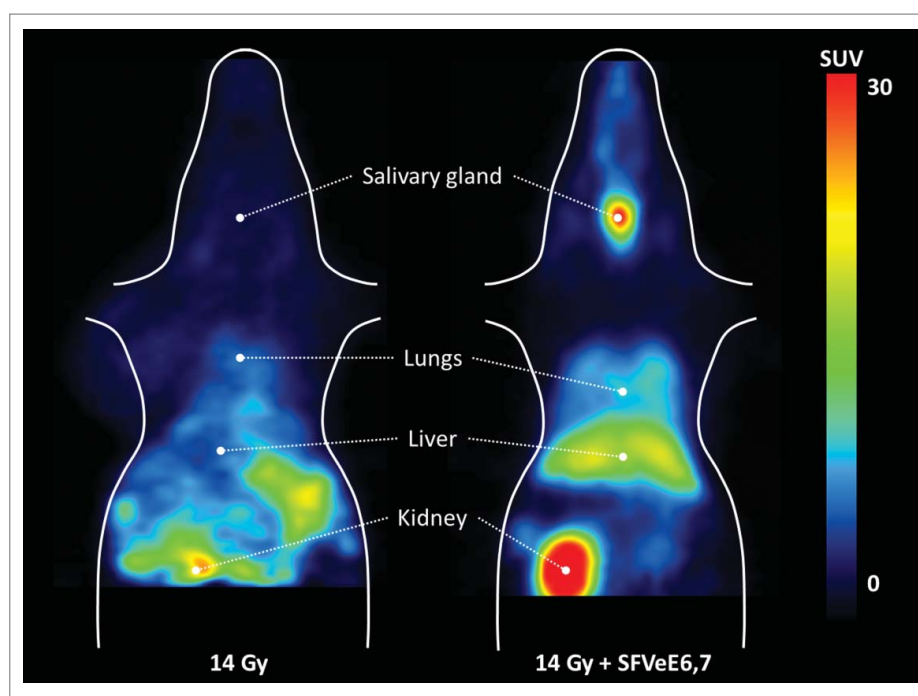
Figure 2. PET images of the tracer distribution in non-target tissues in a mouse treated with local tumor irradiation (left) and local tumor irradiation combined with immunization (right). The animals were placed in the PET camera with the bladder just outside the field-of-view to avoid artifacts due to the high amount of radioactivity in the urine.

increased 2.7-fold (9.1 $\pm$ 2.7 %ID/g), compared with the group treated with irradiation alone ($p < 0.001$) and approximately 27-fold compared with the non-irradiated control group ($p < 0.001$, Fig. 1F). Interestingly, the combination of tumor irradiation and immunization not only affected the tracer uptake in the tumor, but also changed the distribution of the tracer in non-target organs (Fig. 2). We further determined the chemotactic mechanism of activated T cell infiltration. To this effect, the chemokine receptor CXCR4, known to mediate lymphocyte migration, was explored using the CXCR4 antagonist, AMD3100. Administration of AMD3100 dampened the tumor infiltration of activated T cells induced by irradiation, as [^{18}F]FB-IL-2 tumor uptake was 2.8-fold decreased in the irradiated and AMD3100 treated group (1.2 $\pm$ 0.6 %ID/g, $p < 0.01$) as compare with the group receiving irradiation alone. Immuno-histochemical staining of frozen tumor tissues with an anti-CD8$^+$ antibody confirmed the highest levels of CD8$^+$ T cells being present within tumors from mice treated with the combination of irradiation and immunization (Fig. S2).

Ex vivo biodistribution was performed to confirm the results of PET imaging and to determine the effect of treatment on the total body distribution of activated T lymphocytes. The *ex vivo* analysis of the excised tumors showed that [^{18}F]FB-IL-2 uptake was approximately 10-fold higher in irradiated tumors (4.9 $\pm$ 1.8 %ID/g) as compare with the sham-irradiated controls (0.47 $\pm$ 0.17 %ID/g, $p < 0.01$). Treatment with local tumor irradiation followed by daily administration of AMD3100 decreased [^{18}F]FB-IL-2 tumor uptake 2.2-fold (2.21 $\pm$ 0.66 %ID/g) compared with irradiation alone ($p < 0.05$). Immunization with SFVeE6,7 further enhanced the irradiation-induced T cell infiltration, as mice receiving combined irradiation and immunization treatment presented a 2.7-fold or 30-fold increase in [^{18}F]FB-IL-2 uptake in the tumor

(13.6 $\pm$ 5.0 %ID/g), compared with the group receiving local tumor irradiation alone ($p < 0.005$) or no treatment at all, respectively ($p < 0.0001$; Fig. 3 and Table 1).

Collection and processing of organs from treated and non-treated tumor-bearing mice allowed us to monitor the *ex vivo* [^{18}F]FB-IL-2 tracer distribution in different organs throughout the body. Local tumor irradiation alone did not significantly enhance tracer uptake in any organ/tissue other than tumor (Fig. 3 and Table 1). Treatment with AMD3100 did not affect tracer uptake in any major organ either, despite increased tracer concentrations in blood and plasma. However, combined treatment with local tumor irradiation and SFVeE6,7 immunization significantly enhanced tracer uptake in immune-related organs, such as spleen (5-fold, $p < 0.001$), salivary gland (5-fold, $p < 0.001$), lymph nodes (6-fold, $p < 0.001$), and bone marrow (7-fold, $p < 0.05$; Fig. 3 and Table 1), as compared mice receiving 14 Gy local tumor irradiation alone. In addition, combined irradiation and immunization resulted in a significantly increased tracer uptake in lungs, thymus ($p < 0.01$), blood, plasma, and liver ($p < 0.05$), when compared with irradiation alone.

In sham-irradiated control animals, the highest levels of radioactivity were observed in the kidney compared with all other organs (22 $\pm$ 11 %ID/g). This is due to the clearance property of the tracer. Plasma tracer analysis by the tricholoro-acetic acid precipitation method suggests that more than 96% of the tracer was still intact at 35 min after tracer injection in all groups (Fig. 4), irrespective of the injected tracer dose. Conversely, urine analysis showed that the tracer was completely metabolized in all groups with the percentage of intact tracer being lower than 3%. These results suggest that the kidney metabolizes the tracer and excretes the metabolites into the
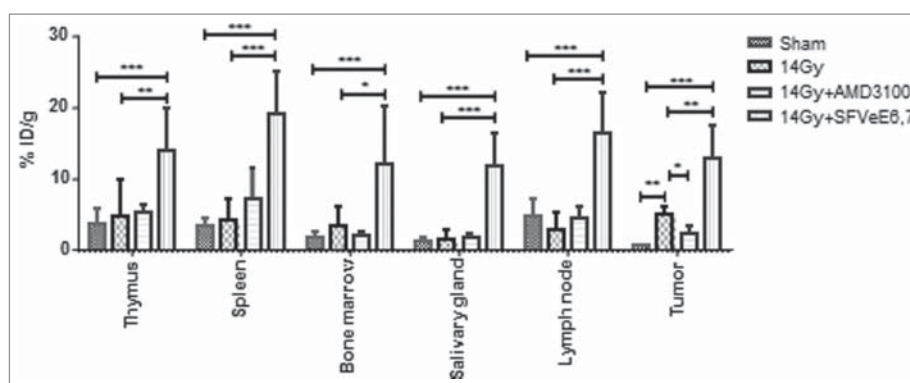
Figure 3. *Ex vivo* biodistribution of [^{18}F]FB-IL-2. *Ex vivo* biodistribution 50 min after injection of [^{18}F]FB-IL-2 in TC-1 tumor bearing C57B/6 mice, irradiated with a single 14 Gy irradiation or sham-irradiated. One group of irradiated mice was treated with AMD3100, whereas another group of irradiated mice was immunized with single dose of 5×10^6 SFVeE6,7 particles. The *ex vivo* quantitative estimation of the tracer uptake is expressed as percentage of the injected dose per gram of tissue (%ID/g). Tracer uptake in the tumor of mice subjected to different treatments and in different immunological organs. All the data represent the mean $\pm$ standard deviation and the statistical difference are indicated by $^*p < 0.05$, $^{**}p < 0.01$, and $^{***}p < 0.001$.

urine. These results are comparable with previously published data and indicate that the tracer behaves similar to native IL-2.[4]

Discussion

In this report, we successfully demonstrated that cancer therapy-induced activated T lymphocyte infiltration can be noninvasively monitored using a radiotracer targeting CD25. We previously reported that the [^{18}F]FB-IL-2 tracer effectively targets CD25 *in vivo*. The binding capacity of [^{18}F]FB-IL-2 was validated as a significant correlation was observed with the number of human CD25$^+$ cells subcutaneously inoculated in Wistar rats within the context of inflammation.[4]

To extend [^{18}F]FB-IL-2 as a diagnostic tool for immune activation, established treatments of local tumor irradiation and rSFVeE6,7 immunization were used, as they synergistically enhance activation of tumor-specific lymphocytes in a preclinical cervical cancer model. We demonstrate a significantly higher [^{18}F]FB-IL-2 uptake in the tumor of mice receiving 14 Gy local tumor irradiation alone or 14 Gy local tumor

irradiation followed by rSFVeE6,7 immunization compare with tumor-bearing mice receiving no treatment. Further validation for expression of CD25 was performed with an *ex vivo* tracer biodistribution analysis of excised tumors. The increase in tumor levels of the tracer compared with the tumor-bearing mice receiving no treatment was 10-fold and 30-fold for irradiation alone or irradiation followed by immunization, respectively.

The synergistic effect of the dual therapy complements that of our previous study using the same cervical cancer model.[7] However, the increase in the number of CD8$^+$ TIL was 10-fold in our previous study, whereas a 30-fold increase in tracer activity was observed in this study.[7] This difference may be accounted for by differences IL-2 receptor levels expressed on activated T cells and by IL-2 receptor expression on other infiltrating lymphocytes, such as natural killer cells. The synergistic increase in tracer accumulation was also observed in immune-related organs. This non-target infiltration may be of crucial importance in predicting immune-related adverse events such as organ toxicity. The dual therapy also induced increased tracer levels in blood and well-perfused organs such as the liver,

Table 1. *Ex vivo* biodistribution of [^{18}F]FB-IL-2 50 min after tracer injection in TC-1 tumor bearing C57B/6 mice treated with sham-irradiation or 14 Gy local tumor irradiation alone or in combination with the CXCR4 antagonist AMD3100 or immunization with SFVeE6,7.

Tissue	14 Gy ($n = 6$)	Sham ($n = 5$)	14 Gy + AMD3100 ($n = 5$)	14 Gy + SFVeE6,7 ($n = 6$)
Total blood	6.23 ± 2.40	7.28 ± 2.52	$20.18 \pm 3.15^*$	$27.29 \pm 5.91^*$
Plasma	14.52 ± 8.03	6.77 ± 1.87	$34.40 \pm 4.36^*$	$45.10 \pm 9.38^*$
Heart	4.58 ± 3.04	2.38 ± 1.24	6.52 ± 1.70	18.55 ± 5.42
Lungs	5.60 ± 2.68	4.15 ± 2.69	4.59 ± 2.63	$27.76 \pm 6.10^{**}$
Thymus	4.68 ± 2.53	3.51 ± 1.77	5.23 ± 1.16	$13.81 \pm 5.91^{**}$
Kidneys	22.08 ± 10.91	21.96 ± 7.24	11.40 ± 3.09	31.89 ± 10.74
Liver	8.30 ± 3.05	8.42 ± 4.22	9.80 ± 2.65	$55.30 \pm 16.51^*$
Pancreas	2.91 ± 0.92	2.56 ± 1.08	1.85 ± 0.13	7.58 ± 2.19
Spleen	4.05 ± 1.23	3.22 ± 1.26	6.99 ± 1.96	$18.89 \pm 6.12^{***}$
Colon	2.19 ± 1.56	1.65 ± 1.22	2.29 ± 0.52	8.60 ± 2.53
Ileum	4.45 ± 1.89	2.55 ± 1.34	3.23 ± 1.36	9.59 ± 2.80
Muscle	2.22 ± 1.94	2.54 ± 1.50	1.20 ± 0.86	4.31 ± 2.13
Bone marrow	3.17 ± 2.76	1.61 ± 0.78	2.01 ± 0.56	$11.83 \pm 6.32^*$
Brain	0.42 ± 0.26	0.30 ± 0.05	0.45 ± 0.13	1.22 ± 0.88
Salivary glands	2.51 ± 1.21	1.26 ± 0.28	1.66 ± 0.44	$11.81 \pm 4.61^{***}$
Lymph nodes	2.78 ± 2.48	4.76 ± 2.31	4.48 ± 1.64	$16.41 \pm 5.60^{***}$
Tumors	4.93 ± 1.76	$0.47 \pm 0.17^{**}$	$2.21 \pm 0.66^*$	$13.62 \pm 5.00^{**}$

[^{18}F]FB-IL-2 tracer uptake was expressed as percentage of injected tracer dose per gram tissue (%ID/g). Data are presented as mean $\pm$ standard deviation. Significant differences between groups and mice that were irradiated with 14 Gy are illustrated by $^*p < 0.05$, $^{**}p < 0.01$, and $^{***}p < 0.001$.
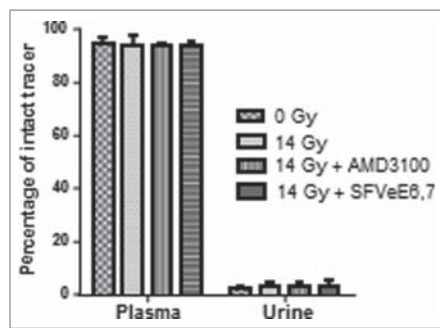
Figure 4. Stability of the tracer [^{18}F]FB-IL-2 in plasma and urine 35 min after injection in different groups. The tracer was found to be >96% stable in plasma and <3% in urine, as analyzed by TCA assay.

brain, and heart. However, radioactivity levels in these organs likely reflect the higher tracer levels in the blood compartment rather than T-cell infiltration. The increased plasma radioactivity levels in immunized animals may also have contributed to the increased tracer uptake in the tumor, as the tumor-to-plasma ratio in irradiated and immunized animals was similar to that in mice that were only irradiated. The increased uptake due to tumor irradiation alone, however, cannot be ascribed to changes in plasma radioactivity levels, as the tumor-to-plasma ratio in sham-treated mice (and in AMD3100-treated mice) were about 5-fold lower than in irradiated mice. Pharmacokinetic modeling could have helped to eliminate any effects of plasma radioactivity levels and perfusion on tumor uptake, as we have shown before.[4] However, this method requires repetitive arterial blood sampling and therefore was not feasible here as the blood volume of mice is too small.

The kidneys showed the highest uptake of the tracer, even in mice that were not treated, because the kidney is the major clearance organ of the tracer. Native IL-2 was proven to be metabolized and excreted by the kidneys.[5,16] As a result of the rapid renal tracer clearance in mice, detection of lesions in or near the kidneys and the bladder will not be possible with [^{18}F]FB-IL-2 PET.

At first glance, PET imaging appears to demonstrate lower tumor uptake of [^{18}F]FB-IL-2 as compared with the *ex vivo* biodistribution. This apparent discrepancy can be explained by underestimation of the absolute amount of radioactivity measured by PET, due to partial volume effects.[17] The average volume of the tumor in this study was 500 mm^3 which corresponds to a diameter that is less than one order of magnitude larger than the spatial resolution of the PET camera (approximately 1.5 mm in the center of the field of view) and consequently the specific tumor signal is partly diluted with the background signal. As partial volume effects are less pronounced in humans than in mice, the novel non-invasive PET method we used in this study should allow simultaneous detection of activated T lymphocyte levels in various organs, such as in spleen and lymph nodes, although some underestimation might still occur in small lesions.

Utilizing [^{18}F]FB-IL-2 PET, we were also able to determine the mechanism of TIL infiltration with the CXCR4 inhibitor AMD3100 (Plerixafor), which is approved as an orphan drug for the mobilization of hematopoietic stem cells in Europe and the USA. In the group receiving irradiation followed by AMD3100 administration, [^{18}F]FB-IL-2 tumor uptake was

significantly lower by 2.8-fold than the group receiving irradiation alone, despite AMD3100-treated animals having higher blood and plasma levels of the tracer. This increase in tracer levels in blood might be due to mobilization of hematopoietic stem cells from bone marrow induced by the drug. To further validate the infiltration of activated T cells in the tumor microenvironment, we performed immunohistochemistry staining for CD8$^+$ cells on frozen tumor tissue. The immunostaining results indicate a correlation of the *in vivo* results with higher infiltration of CD8$^+$ T cells upon dual treatment and lower infiltration with CXCR4 blockade. These data suggest that radiation-induced tumor infiltration of activated T cells is at least partly regulated by CXCR4-mediated chemotaxis. CXCR4 is constitutively expressed on the surface of murine cytotoxic T cells and specific peptide immunization of immunocompetent wild-type mice has been shown to cause a preferential upregulation of CXCR4 on the surface of CD8$^+$ T cells.[18,19]

Particular immunotherapeutic strategies that gained momentum in recent years include monoclonal antibodies as immune checkpoint inhibitors. The success of monoclonal antibodies directed against programmed cell death protein 1 (PD1) (Nivolumab, Bristol-Myers Squibb) for instance is reflected by the delayed progression-free survival of late stage melanoma patients.[20] However, due to the high costs and delayed response, there is a pressing need to select patient that could potentially benefit from this therapy. For this purpose, researchers have employed immunoPET for non-invasive visualization of antibodies, either within the context of PD-1 or CD8$^+$-expressing lymphocytes.[21-24] ImmunoPET technology offers the advantage of gaining insight into the biodistribution of therapeutic antibodies and hence determining the outcome of antibody-based immunotherapy. Despite this, the imaging method presents with the limitation of the slow kinetics and target binding of labeled antibodies, which requires the use of radio-isotopes with a long half-life (e.g., ^{89}Zr and ^{124}I), associated with a high radiation burden to the patient (~20 mSv for a typical dose of 37 MBq).[25] This can restrict repeated measurements (e.g., baseline vs. follow-up) and precludes monitoring of fast dynamic processes. The use of tracers with faster kinetics labeled with a short-lived isotope can circumvent this limitation. Radu et al. proposed the nucleoside [^{18}F]FAC, a substrate of deoxycytidine kinase, as a new probe for imaging of the deoxyribonucleotide salvage pathway and were able to show immune activation and suppression in mice with this probe.[26] The specificity of this approach, however, remains to be determined, as the salvage pathway may also be activated in tumors. A more specific approach may be the use of small antibody fragments targeting a cell type-specific marker, as was shown by Blykers et al., who labeled antibody fragments against the mannose receptor with ^{18}F to image M2-type macrophages.[27] A similar strategy can be followed by labeling specific cytokines like IL-2. [^{18}F]FB-IL-2 shows rapid clearance and high binding affinity of the cytokine to its receptor and therefore seems a suitable marker for a "dynamic" process as inflammation for effective antitumor control and provides rather mechanistic information of the applied therapies. However, ideally one may consider combining strategies for optimal assessment of treatment efficacy.

In conclusion, this proof-of-concept report brings forth [^{18}F]FB-IL-2 PET as a clinical biomarker to monitor treatment-induced whole-body infiltration of activated T lymphocytes and, on that basis, guide the scheduling and monitoring of novel cancer immunotherapeutics.

Disclosure of potential conflicts of interest

H.W. Nijman and T. Daemen are stock holders/founders of ViciniVax, a spin-off company of the UMCG, developing cancer vaccines.

ORCID

V. Manuelli [ID] http://orcid.org/0000-0002-7996-4835
E. F. J. de Vries [ID] http://orcid.org/0000-0002-6915-1590

References

1. Klebanoff CA, Acquavella N, Yu Z, Restifo NP. Therapeutic cancer vaccines: are we there yet? Immunol Rev 2011; 239:27-44; PMID:21198663; http://dx.doi.org/10.1111/j.1600-065X.2010.00979.x
2. Rosenberg SA. Decade in review-cancer immunotherapy: entering the mainstream of cancer treatment. Nat Rev Clin Oncol 2014; 11:630-2; PMID:25311350; http://dx.doi.org/10.1038/nrclinonc.2014.174
3. Bayer AL, Pugliese A, Malek TR. The IL-2/IL-2R system: from basic science to therapeutic applications to enhance immune regulation. Immunol Res 2013; 57:197-209; PMID:24214027; http://dx.doi.org/10.1007/s12026-013-8452-5
4. Di Gialleonardo V, Signore A, Willemsen AT, Sijbesma JW, Dierckx RA, de Vries EF. Pharmacokinetic modelling of N-(4-[(18)F]fluorobenzoyl)interleukin-2 binding to activated lymphocytes in an xenograft model of inflammation. Eur J Nucl Med Mol Imaging 2012; 39:1551-60; PMID:22777334; http://dx.doi.org/10.1007/s00259-012-2176-y
5. Di Gialleonardo V, Signore A, Glaudemans AW, Dierckx RA, De Vries EF. N-(4-18F-fluorobenzoyl)interleukin-2 for PET of human-activated T lymphocytes. J Nucl Med 2012; 53:679-86; PMID:22499614; http://dx.doi.org/10.2967/jnumed.111.091306
6. Daemen T, Riezebos-Brilman A, Bungener L, Regts J, Dontje B, Wilschut J. Eradication of established HPV16-transformed tumours after immunisation with recombinant Semliki Forest virus expressing a fusion protein of E6 and E7. Vaccine 2003; 21:1082-8; PMID:12559783; http://dx.doi.org/10.1016/S0264-410X(02)00558-3
7. Draghiciu O, Walczak M, Hoogeboom BN, Franken KL, Melief KJ, Nijman HW, Daemen T. Therapeutic immunization and local low-dose tumor irradiation, a reinforcing combination. Int J Cancer 2014; 134:859-72; PMID:23922012; http://dx.doi.org/10.1002/ijc.28418
8. Lugade AA, Moran JP, Gerber SA, Rose RC, Frelinger JG, Lord EM. Local radiation therapy of B16 melanoma tumors increases the generation of tumor antigen-specific effector cells that traffic to the tumor. J Immunol 2005; 174:7516-23; PMID:15944250; http://dx.doi.org/10.4049/jimmunol.174.12.7516
9. Matsumura S, Demaria S. Up-regulation of the pro-inflammatory chemokine CXCL16 is a common response of tumor cells to ionizing radiation. Radiat Res 2010; 173:418-25; PMID:20334513; http://dx.doi.org/10.1667/RR1860.1
10. Sharma A, Bode B, Wenger RH, Lehmann K, Sartori AA, Moch H, Knuth A, von Boehmer L, van den Broek M. γ-Radiation promotes immunological recognition of cancer cells through increased expression of cancer-testis antigens in vitro and in vivo. PLoS One 2011; 6:e28217; PMID:22140550; http://dx.doi.org/10.1371/journal.pone.0028217
11. Gameiro SR, Jammeh ML, Wattenberg MM, Tsang KY, Ferrone S, Hodge JW. Radiation-induced immunogenic modulation of tumor enhances antigen processing and calreticulin exposure, resulting in enhanced T-cell killing. Oncotarget 2014; 5:403-16; PMID:24480782; http://dx.doi.org/10.18632/oncotarget.1719
12. Apetoh L, Ghiringhelli F, Tesniere A, Criollo A, Ortiz C, Lidereau R, Mariette C, Chaput N, Mira JP, Delaloge S et al. The interaction between HMGB1 and TLR4 dictates the outcome of anticancer chemotherapy and radiotherapy. Immunol Rev 2007; 220:47-59; PMID:17979839; http://dx.doi.org/10.1111/j.1600-065X.2007.00573.x
13. Suzuki Y, Mimura K, Yoshimoto Y, Watanabe M, Ohkubo Y, Izawa S, Murata K, Fujii H, Nakano T, Kono K. Immunogenic tumor cell death induced by chemoradiotherapy in patients with esophageal squamous cell carcinoma. Cancer Res 2012; 72:3967-76; PMID:22700877; http://dx.doi.org/10.1158/0008-5472.CAN-12-0851
14. Lin KY, Guarnieri FG, Staveley-O'Carroll KF, Levitsky HI, August JT, Pardoll DM, Wu TC. Treatment of established tumors with a novel vaccine that enhances major histocompatibility class II presentation of tumor antigen. Cancer Res 1996; 56:21-6; PMID:8548765
15. Daemen T, Riezebos-Brilman A, Regts J, Dontje B, Van Der Zee A, Wilschut J. Superior therapeutic efficacy of alphavirus-mediated immunization against human papilloma virus type 16 antigens in a murine tumour model: effects of the route of immunization. Antivir Ther 2004; 9:733-42; PMID:15535411
16. Donohue JH, Rosenberg SA. The fate of interleukin-2 after in vivo administration. J Immunol 1983; 130:2203-8; PMID:6601147
17. Soret M, Bacharach SL, Buvat I. Partial-volume effect in PET tumor imaging. J Nucl Med 2007; 48:932-45; PMID:17504879; http://dx.doi.org/10.2967/jnumed.106.035774
18. Schabath R, Müller G, Schubel A, Kremmer E, Lipp M, Förster R. The murine chemokine receptor CXCR4 is tightly regulated during T cell development and activation. J Leukoc Biol 1999; 66:996-1004; PMID:10614783
19. Baggiolini M. Chemokines and leukocyte traffic. Nature 1998; 392:565-8; PMID:9560152; http://dx.doi.org/10.1038/33340
20. Topalian SL, Sznol M, McDermott DF, Kluger HM, Carvajal RD, Sharfman WH, Brahmer JR, Lawrence DP, Atkins MB, Powderly JD et al. Survival, durable tumor remission, and long-term safety in patients with advanced melanoma receiving nivolumab. J Clin Oncol 2014; 32:1020-30; PMID:24590637; http://dx.doi.org/10.1200/JCO.2013.53.0105
21. Maute RL, Gordon SR, Mayer AT, McCracken MN, Natarajan A, Ring NG, Kimura R, Tsai JM, Manglik A, Kruse AC et al. Engineering high-affinity PD-1 variants for optimized immunotherapy and immuno-PET imaging. Proc Natl Acad Sci USA 2015; 112:E6506-14; PMID:26604307; http://dx.doi.org/10.1073/pnas.1519623112
22. Natarajan A, Mayer AT, Xu L, Reeves RE, Gano J, Gambhir SS. Novel radiotracer for ImmunoPET imaging of PD-1 checkpoint expression on tumor infiltrating lymphocytes. Bioconjug Chem 2015; 26:2062-2069; PMID:26307602; http://dx.doi.org/10.1021/acs.bioconjchem.5b00318
23. Tavare R, Escuin-Ordinas H, Mok S, McCracken MN, Zettlitz KA, Salazar FB, Witte ON, Ribas A, Wu AM. An effective immuno-PET imaging method to monitor CD8-dependent responses to immunotherapy. Cancer Res 2015; 76:73-82; PMID:26573799; http://dx.doi.org/10.1158/0008-5472.CAN-15-1707
24. Tavaré R, McCracken MN, Zettlitz KA, Salazar FB, Olafsen T, Witte ON, Wu AM. Immuno-PET of murine t cell reconstitution

postadoptive stem cell transplantation using anti-CD4 and anti-CD8 Cys-diabodies. J Nucl Med 2015; 56:1258-64; PMID:25952734; http://dx.doi.org/10.2967/jnumed.114.153338

25. Makris NE, Boellaard R, van Lingen A, Lammertsma AA, van Dongen GA, Verheul HM, Menke CW, Huisman MC. PET/CT-derived whole-body and bone marrow dosimetry of 89Zr-cetuximab. J Nucl Med. 2015; 56:249-54; PMID:25613538; http://dx.doi.org/10.2967/jnumed.114.147819

26. Radu CG, Shu CJ, Nair-Gill E, Shelly SM, Barrio JR, Satyamurthy N, Phelps ME, Witte ON. Molecular imaging of lymphoid organs and immune activation by positron emission tomography with a new [18F]-labeled 2'-deoxycytidine analog. Nat Med. 2008; 14:783-8; PMID:18542051; http://dx.doi.org/10.1038/nm1724

27. Blykers A, Schoonooghe S, Xavier C, D'hoe K, Laoui D, D'Huyvetter M, Vaneycken I, Cleeren F, Bormans G, Heemskerk J et al. PET imaging of macrophage mannose receptor-expressing macrophages in tumor stroma using ^{18}F-radiolabeled camelid single-domain antibody fragments. J Nucl Med. 2015; 56:1265-71; PMID:26069306; http://dx.doi.org/10.2967/jnumed.115.156828